



Electron pair emission from a Cu(111) surface upon photon absorption

F. O. Schumann, N. Fominykh, C. Winkler, and J. Kirschner
Max-Planck Institut für Mikrostrukturphysik, Weinberg 2, 06120 Halle, Germany

J. Berakdar

*Institut für Physik, Martin-Luther-Universität Halle-Wittenberg, Nanotechnikum-Weinberg, Heinrich-Damerow-St. 4,
 06120 Halle, Germany*

(Received 6 February 2008; revised manuscript received 7 April 2008; published 24 June 2008)

We studied the electron pair emission from a Cu(111) surface upon photon absorption. We found that the energy sharing depends on the angle between the trajectories of the two emitted electrons. The angular distribution of the coincidence intensity displays a zone of reduced intensity, if the emission direction of one electron is fixed. We are able to observe the full extension and shape of this depletion zone. It has an angular extension of ≈ 1.2 rad, which is independent of the electron energy. This depletion zone is a manifestation of the exchange-correlation hole. The experimental results are discussed in connection with a detailed theoretical description.

DOI: [10.1103/PhysRevB.77.235434](https://doi.org/10.1103/PhysRevB.77.235434)

PACS number(s): 79.60.-i, 73.20.At

I. INTRODUCTION

Electrons will not move independently through a solid but will experience a mutual influence in their motion, which is mediated by the Coulomb interaction and the Pauli principle. This leads to an important concept of solid theory, namely, the exchange-correlation (xc) hole,¹⁻³ which states that electrons tend to stay away from each other. This creates a zone of reduced electronic charge around each electron. The mutual influence among electrons is ultimately responsible for many-body effects in samples, which display magnetism, superconductivity, heavy fermions, etc. These “highly correlated” systems are the focus of intense research activities. The electronic properties of solids can be accessed via photoemission. In particular, angle-resolved energy distributions allow comparison with band structure calculations. Usually, one discusses peaks in the intensity distributions within an effective single-electron picture. Recent advances in the angle and energy resolution have made it possible that photoemission allows us to observe the effects due to many-body interactions. These so-called kinks in the $E(k)$ curve are the result of the electron-electron (ee) interaction or the coupling to other degrees of freedom.⁴ An alternative way to investigate the electron-electron interaction in solids is offered by the technique of double photoemission (DPE) or $(\gamma, 2e)$, which is the absorption of a single photon followed by the simultaneous emission of an electron pair. Within the dipole approximation a noninteracting electron system has a vanishing DPE intensity, therefore a finite DPE intensity requires a finite electron-electron interaction.⁵ The possibility to probe the xc hole via DPE exists, as a theoretical treatment for a Cu(100) surface showed.⁶ This is beyond the capabilities of single photoemission. The experimental possibility to detect a finite DPE intensity from solids has been demonstrated previously.⁷⁻¹¹

In this work we present our experimental results on the double photoemission from a Cu(111) surface. We will show that the angle between the trajectories of the two emitted electrons determines how the photon energy is shared. Fur-

thermore we will demonstrate that the complete mapping of the xc hole is possible.

II. EXPERIMENT

In Fig. 1 we provide a schematic view of our time-of-flight experimental setup and the two geometries employed. Our experiment consists basically of three channel-plate detectors. If the incident photon beam is parallel to the surface normal, we use two of these [see Fig. 1(a)]. For this symmetric arrangement the angular acceptance is $\pm 55^\circ$ in the drawing plane and $\pm 20^\circ$ perpendicular to it. The second geometry, for an angle of 32° of the photon beam with respect to the surface normal, has an increased angular acceptance of $\pm 90^\circ$ in the drawing plane [Fig. 1(b)]. Delay line anodes allow the determination of the impact positions of the electrons. It is possible to recover the impact positions of coincident pairs even if they hit the same detector. These events we may term “double hits,” whereas we refer to “single hits,” if the electrons are registered on different detectors. Further details of the experimental setup can be found elsewhere.¹² As a pulsed photon source serves the BESSY storage ring operating in the single bunch mode at beamline TGM 4. The data to be presented have been obtained during the maximum available single bunch time of a year, which amounts to about 20 days. Therefore only one photon energy could be selected, which was set to $\hbar\omega = 50 \pm 0.2$ eV. The polarization plane of the linear polarized light is in the drawing plane (see Fig. 1). The electron energies are determined via the flight times, where the BESSY bunch marker is taken as the time reference. The total time resolution is approximately 1.4 ns. This will lead to an energy dependent energy resolution, which is 1.5 eV for 20 eV electrons. A low kinetic-energy cutoff is provided by a retarding mesh right in front of each channel plates. A grounded mesh placed immediately in front of this retarding mesh ensures a field-free region along the flight path. A coincidence circuit ensures that only electron pairs are detected. The spectrometer is part of an ultrahigh

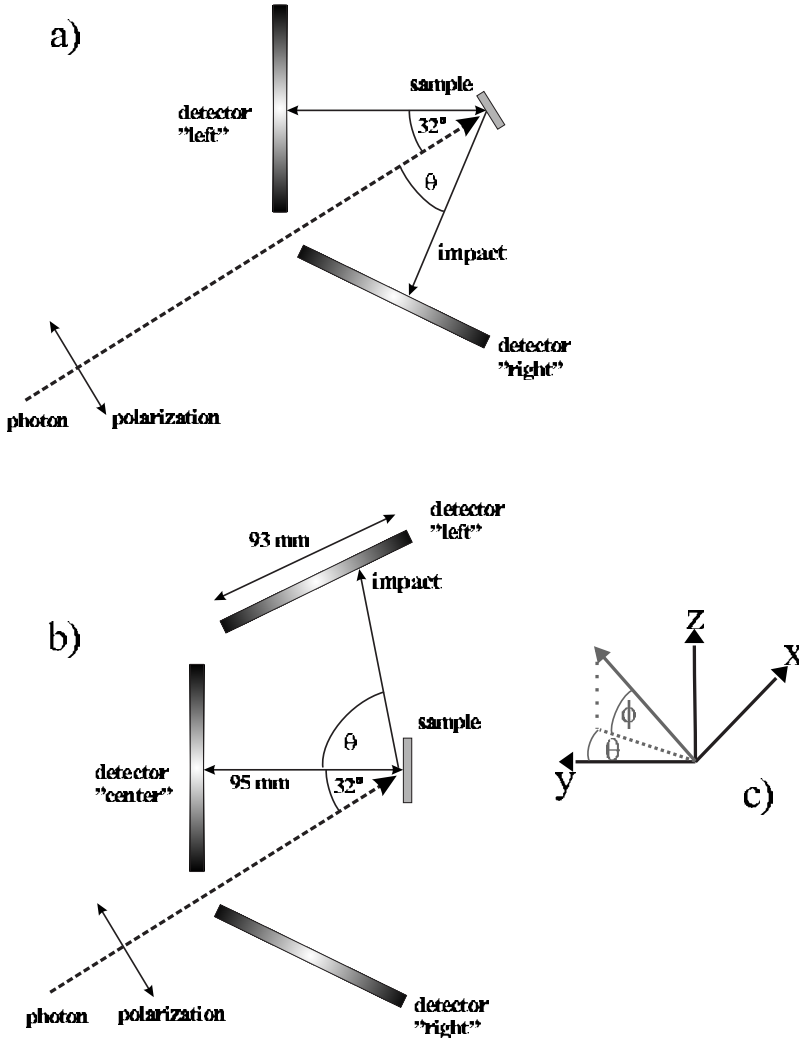


FIG. 1. Schematic view of the experiment and the two different geometries used. The polarization plane of the linear polarized light is in the drawing plane. The photon energy was set to 50 ± 0.2 eV.

vacuum system equipped with standard surface science tools. We define a coordinate system, which has the origin at the sample surface [see Fig. 1(c)]. The y axis is always parallel to the surface normal, whereas the x and z directions are in the surface plane and are orthogonal to each other. Specifically the crystallographic $[\bar{2}11]$ direction is in the drawing plane of Fig. 1, which we define to be the x axis. In order to specify the emission direction of the electrons, we compute the two in-plane components of the momentum. In order to compare the emission directions of electrons with different kinetic energies, we finally calculate the normalized components of the in-plane momentum. These are nothing but the directional cosines, which we label by X and Z , respectively. Each coincident event is then characterized by six coordinates, namely, the individual energies and the individual values of X and Z . We studied a clean and well-ordered Cu(111) surface, which was prepared via Ar sputtering and annealing up to 800 K. The experiments were performed at room temperature. Prior to the discussion of the data, a few technical aspects have to be clarified. As defined above, single hits constitute events where for example one electron is registered on the “left” detector, whereas the other hits the “center” or “right” detector. In this case there is a well-defined way to label the electrons, namely, according to the detector

they hit. It is obvious that this cannot be extended to double hits, since both electrons would get the same label. This leaves certain arbitrariness for plotting the data. This can be avoided if we use a label of either “fast” or “slow” where the distinction comes from the difference in the kinetic energy, namely, $E_{\text{fast}} > E_{\text{slow}}$. Since we want to combine double hits and single hits, we employ the same labeling for the latter, too. Another important aspect is the fact that the detection of double hits with the same kinetic energy is not possible.

III. DOUBLE PHOTOEMISSION IN NORMAL INCIDENCE

In our presentation we start with the experimental results obtained with normal incidence of the photons. As described in the experimental part, we use two detectors in this case, which we may label left and right, respectively. We further consider only single hits, this means only coincidence events where the two electrons hit different detectors are registered. In Fig. 2 we plot the coincidence intensity as a function of the sum energy $E_{\text{sum}} = E_{\text{left}} + E_{\text{right}}$. The vertical dashed line marks the energy position of the maximum sum energy $E_{\text{max}} = 40$ eV imposed by energy conservation, since the work function of the Cu(111) surface (≈ 5 eV) has to be

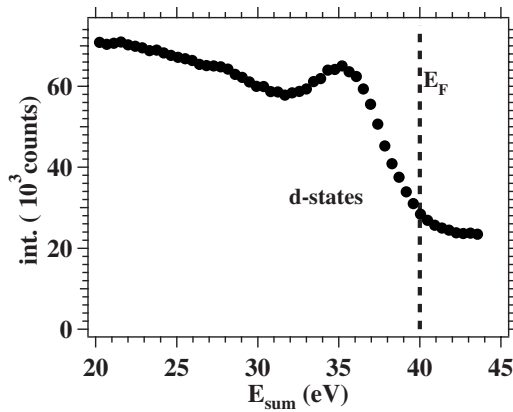


FIG. 2. Plot of the E_{sum} distribution of the $(\gamma, 2e)$ experiment. The vertical dashed line is the energy position of the highest possible sum energy, which follows from energy conservation. A pronounced emission at 35 eV can be noticed.

subtracted twice from the photon energy of 50 eV. It is apparent that the pair emission is governed by a contribution located at $E_{\text{sum}} \approx 35$ eV. We recall that the center of gravity of the Cu 3d band is roughly 2.5 eV below the Fermi level E_F , hence we identify the peak at 35 eV with the pair emission from the Cu 3d bands. It is well known that the Cu(111) surface possesses also a Shockley surface state at the $\bar{\Gamma}$ point.¹³ This state is energetically located in the interval E_F and $E_F - 0.4$ eV. From Fig. 2 we conclude that with the present apparatus and its current limited resolution it is not possible to identify the emission from the surface state. The data shown in Fig. 2 is derived from an integration over the whole accessible angular range, even though the shape of the spectrum has a weakly angular dependence. The background of the intensity distribution of Fig. 2 and its extension above $E_{\text{sum}} = 40$ eV is related to so-called random coincidences. The emission of a single photoelectron is significantly more likely (by a factor of $\approx 10^3$) than the emission of an electron pair upon absorption of a single photon. If a pulse containing two photons hits the sample, the emission of two single photoelectrons is possible. The coincidence logic cannot discriminate between these events and genuine pair emission. The only option one has is to lower the primary intensity, which in turn (due to the Poisson statistics) will increase the probability of finding one photon in a pulse compared to more than one. Two single photoelectrons are not correlated since they originate from two independent excitation processes. For single photoelectrons, energy conservation has to hold, too. This means that the maximum kinetic energy with respect to the vacuum level is the photon energy minus the work function. In our case this amounts to a maximum value of 45 eV. The maximum sum energy of an uncorrelated pair amounts to twice the value. This means if a E_{sum} spectrum is plotted, the intensity can extend up to 90 eV. Of course a genuine electron pair for our experimental conditions cannot have an energy beyond 40 eV.

In Fig. 3 we display the hit pattern of the individual electrons of coincident pairs as a function of the normalized in-plane momentum (or directional cosine). One interesting aspect is how the available energy is shared between the

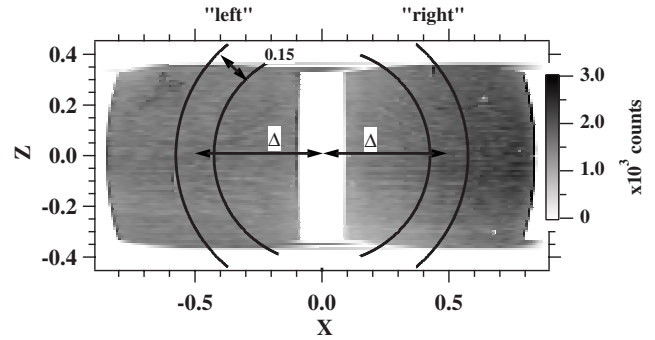


FIG. 3. The hit pattern of electron pairs is displayed. As axes, we use the components of the normalized in-plane momentum of the individual electrons. The excitation was via 50 eV photons, which hits the sample along the surface normal. The pair of arcs on the left and right detector. The gray scale on the right displays the intensity in counts.

electrons, in particular, if we impose geometric constraints. In order to address this point we select regions on the detectors left and right whose boundaries are given by the pair of arcs. The width of these regions is 0.15, and the centers have a distance to the origin given by the value of $|\Delta|$. We ask now how the energy of the two ejected electrons is distributed. This is best done by using a two-dimensional (2D) representation, where the axes are the individual kinetic energies. This we call in the following a 2D energy distribution. The result is shown in Fig. 4 for $\Delta = 0.2$ and $\Delta = 0.7$, respectively. Converted into angles, we constrain the mean angle between the trajectories to be either 23° or 89° , respectively. The dashed diagonal lines in both plots indicate the position of those events, which has a sum energy of 35 eV. We recall from Fig. 2 that at this energy a prominent pair emission occurs. In panel (a) we observe for $\Delta = 0.2$ a boomeranglike distribution. The onset of pair emission at $E_{\text{sum}} = 40$ eV occurs for very unequal energies, which means one of the electrons carries most of the energy. This preference of one electron being fast while the other is slow also occurs for decreasing sum energy. In general the coincidence intensity increases if E_{sum} decreases. The situation for $\Delta = 0.7$ is different as inspection of Fig. 4(b) shows. The onset of pair emission at around $E_{\text{sum}} = 40$ eV is not confined to those electrons that have very unequal energies but occurs for all energy combinations with very similar probability. If we reduce E_{sum} to 35 eV, we note that the intensity remains constant for as long as the energies are outside the regions $20 < E_{\text{left/right}} < 30$ eV and $E_{\text{right/left}} < 10$ eV. From these observations we learn that the prominent emission at $E_{\text{sum}} = 35$ eV occurs for unequal energy sharing and preferably for large values of Δ . In other words the trajectories of the electrons have a large angle. We can emphasize the point if we compute the so-called sharing functions. For a given value of E_{sum} one computes the coincidence intensity as a function of $E_{\text{left}} - E_{\text{right}}$, which is done for $\Delta = 0.2$ and $\Delta = 0.7$ while keeping the sum energy fixed at 35 eV, which defines the pair emission from the 3d states. We allowed an uncertainty of 3 eV, which reflects the width of the peak at $E_{\text{sum}} = 35$ eV. The resulting graph is shown in Fig. 5. These sharing curves will be discussed further in the theoretical section.

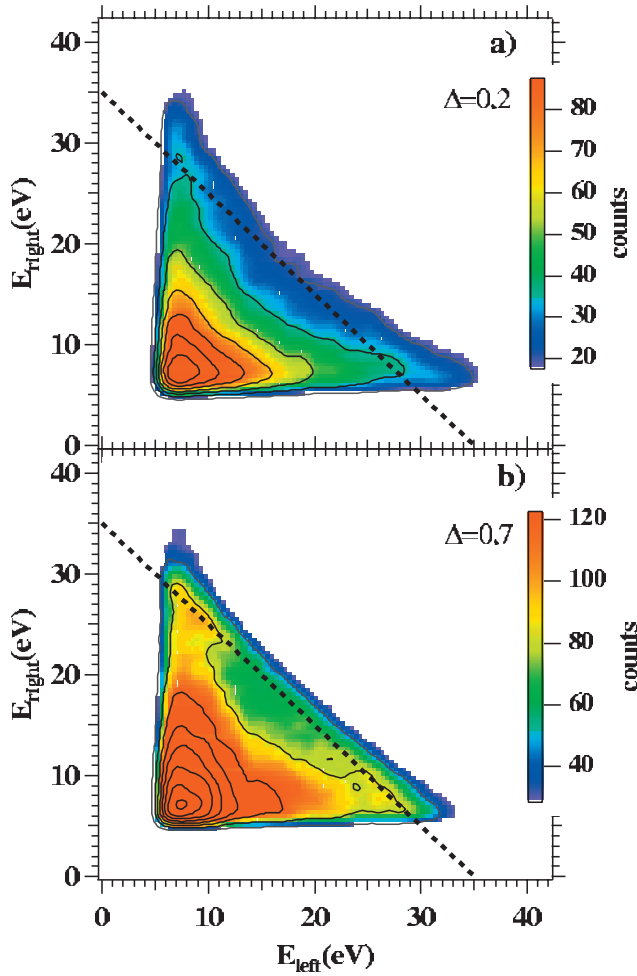


FIG. 4. (Color) 2D energy distributions for $\Delta=0.2$ in (a) and $\Delta=0.7$ in (b). The intensity is given in counts. We added equidistant contours and employed a Gaussian filter. The dashed diagonal line in both plots indicates the emission at $E_{\text{sum}}=35 \text{ eV}$.

IV. 2D MOMENTUM CONTRIBUTIONS

In this section we want to discuss momentum distributions of the coincidence intensity. More specifically, we want to know what impact a fixed emission direction of one electron has on the momentum distribution of the other electron. For this we used the geometry where the incident photon has an angle of 32° with respect to the normal [see Fig. 1(b)]. This mode also includes the detection of double hits, which are events where both electrons are registered on the same detector. A first hint of the angular distribution can be obtained by an inspection of the 2D energy distributions, which we discuss separately for single and double hits. For the latter the angle between the trajectories of the electron are confined to values between 0° and $\approx 52^\circ$. For single hits the angle can be up to 180° . With this in mind we display the 2D energy distributions in Fig. 6 as a function of E_{fast} and E_{slow} . As a guide to the eye, we added contour lines to both plots representing equidistant levels. In the case of double hits these contour lines surround areas that are elongated along the x axis. Most of the intensity is confined in an area, for which E_{slow} is below 7 eV. Contrary to this the fast electron

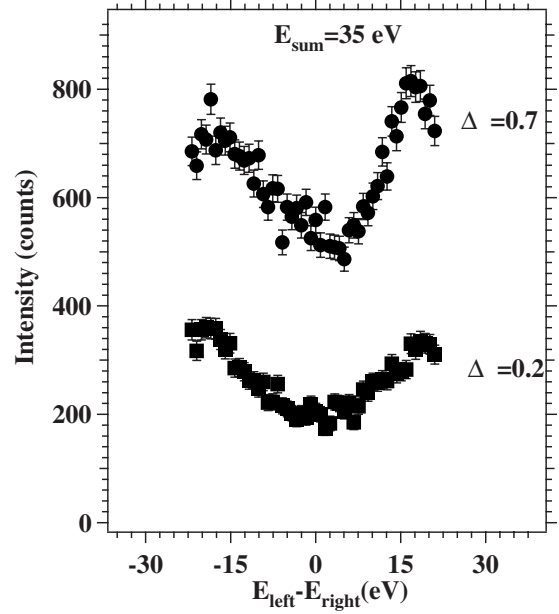


FIG. 5. Sharing curves for $E_{\text{sum}}=35 \pm 1.5 \text{ eV}$ and $\Delta=0.7$. Due to the low kinetic-energy cutoff of 5 eV, the sharing $E_{\text{left}}-E_{\text{right}}$ is in the interval $\pm 23.5 \text{ eV}$.

can have any value consistent with energy conservation. This unequal energy sharing was also observed in Fig. 4(a) although it was not as pronounced. We recall that the geometrical constraint imposed onto the trajectories ($\Delta=0.2$) amounts to an average angle of about 46° . Clearly for double hits, the trajectories are closer on average. From this we learn that the smaller the angle between trajectories the more pronounced the unequal energy sharing becomes.

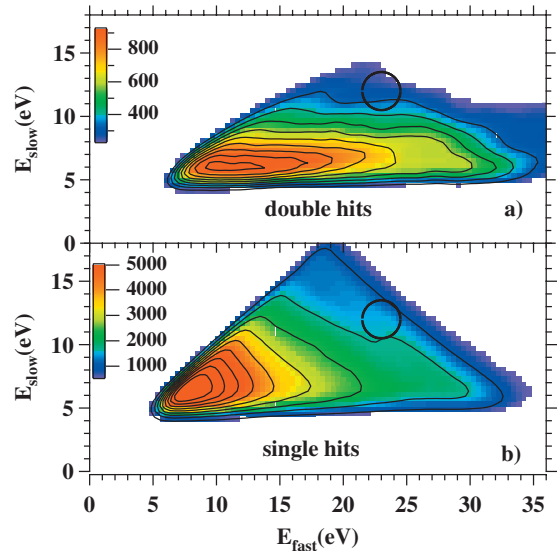


FIG. 6. (Color) 2D energy distribution of coincidence events from a Cu(111) surface excited with 50 eV photons. Panel (a) includes only double hits, in panel (b) we show single hits. Events, which have electron energies that fall into the circle located at $E_{\text{fast}}=23 \text{ eV}$ and $E_{\text{slow}}=12 \text{ eV}$, will be used for angular distributions. We added equidistant contours and employed a Gaussian filter. The color coding for the intensity is given in counts.

If we look at the 2D energy distribution for single hits, a different picture emerges. The intensity level is about a factor of five higher compared to the double hits. This in retrospect justifies that the omission of double hits in the normal incidence geometry was warranted. Since we know that the trajectories for single hits can be up to 180° , we learn that electrons prefer to avoid each other. This statement will be confirmed and discussed more in details below. Apart from the intensity levels, we also note a different distribution of the coincidence intensity for single hits. Unlike the double hits a very unequal energy sharing is not present. Here the contour lines surround more triangular areas. Similar to the situation depicted in Fig. 4(b), we note a drop in intensity if the electron energies are becoming more equal. After the discussion of the energy distributions, we move on to the momentum distribution of the coincidence intensity. In order to facilitate comparison of electrons with different energies, we will use the normalized in-plane components (or directional cosine). These we will label with X and Z , respectively. We obtain the momentum distributions if we execute the following steps. First we select energies of the fast and slow electron, sufficient statistics require that the selected energies include also those events, where the energies are within 1.5 eV of the chosen values. After this step is completed, we obtain the 2D momentum distributions of the fast and slow electron. These are not independent of each other, we emphasize that every fast electron has a slow counterpart. In Fig. 7(a) and 7(b) the distributions for fast and slow electrons centered at $E_{\text{fast}}=23$ eV and $E_{\text{slow}}=12$ eV are plotted. The intensity is given in counts and the color code is on the right-hand side of the plot. Both distributions display intensity in the forward direction, which increases if the momentum increases. It is now interesting to look only at those events where the fast electron is detected in a narrow region. Such a constraint is indicated by the circle displayed in Fig. 7(a), which has a radius of 0.15 around the origin. One can rephrase this by saying that we fix the emission direction of the fast electron and ask for the intensity of the slow electron around this direction. The result is displayed in Fig. 7(c) after normalization to the intensity of the slow electron in Fig. 7(a). Varying detection efficiencies demand such a procedure. It is very clear that the intensity on the center detector is lower than on the left and right detectors. The coincidence intensity has a minimum, which is centered around $X=0$. The minimum is rather broad and only for $|X|>0.4$ the coincidence intensity starts to increase. At around $|X|>0.8$ the intensity starts to saturate. We can state that the slow electron tends to avoid the fast electron, which is the experimental proof of the existence of the xc hole. This is in line with our previous observations where we performed DPE measurements on a NaCl(100) surface.¹¹ The instrument used at the time had an angular acceptance of 34° . If we convert this into directional cosine, the value is 0.55. With this instrument we were able to observe the central part of the xc hole but could not see a saturation of the coincidence intensity for large momentum values. In other words, we were not able to determine the full size of the xc hole. However, our new instrument has a larger acceptance angle and that makes it possible to determine the full extent. It is of course possible to fix the direction of the slow electron and determine the

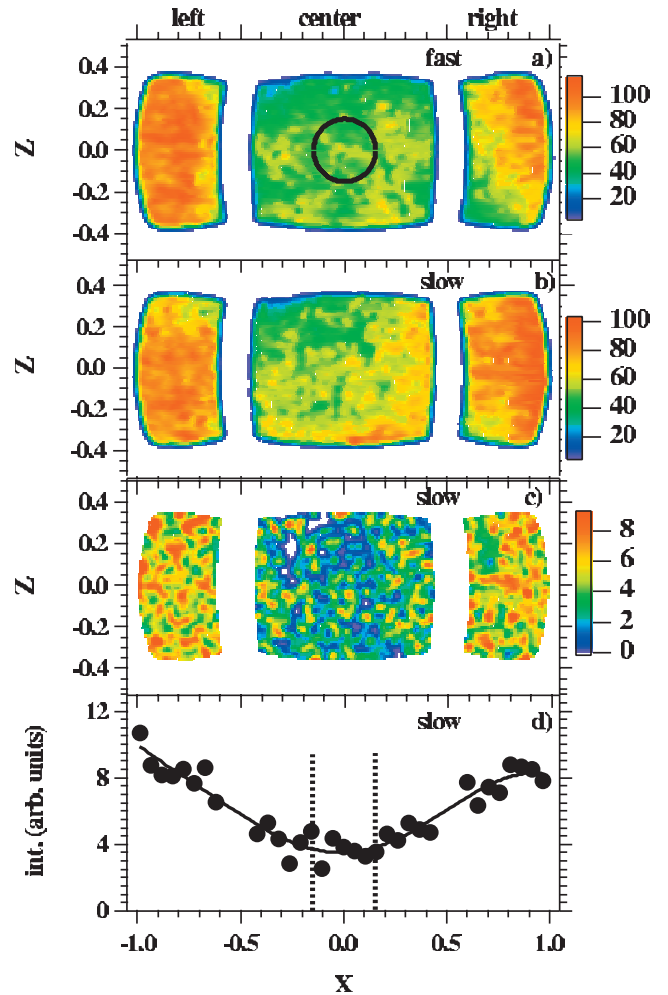


FIG. 7. (Color) The panels display the following distributions, where the electrons have the energies $E_{\text{slow}}=12 \pm 1.5$ eV and $E_{\text{fast}}=23 \pm 1.5$ eV, respectively: Panels (a)–(c) shows 2D distributions of the coincidence intensity where the axes are the components of the normalized in-plane momentum. In panel (a) we plot the for the fast electron, whereas in panel (b) the same for the slow electron is plotted. In panel (c) we plot the intensity for the slow electron if the fast electron is constrained to be within the area defined by the black circle of drawn in panel (a). The color coding indicates the intensity measured in counts. Panel (d) is the intensity profile obtained from (c) upon integrating the intensity for all Z values for a given value of X .

intensity map of the fast electron. The result of such a presentation is qualitatively and quantitatively identical as far as the size and shape of the xc hole is concerned.

V. THEORETIC DESCRIPTION

In this section we analyze our data from a theoretical point of view. For the calculation of the $(\gamma, 2e)$ spectra of the Cu(111) surface, we employ the correlated two-particle layer Korringa-Kohn-Rostoker method that we described in details elsewhere.^{6,14–17} In brief description, two *ab initio* computed single-particle electronic states are coupled via the exchange and the screened Coulomb interaction. The latter is approxi-

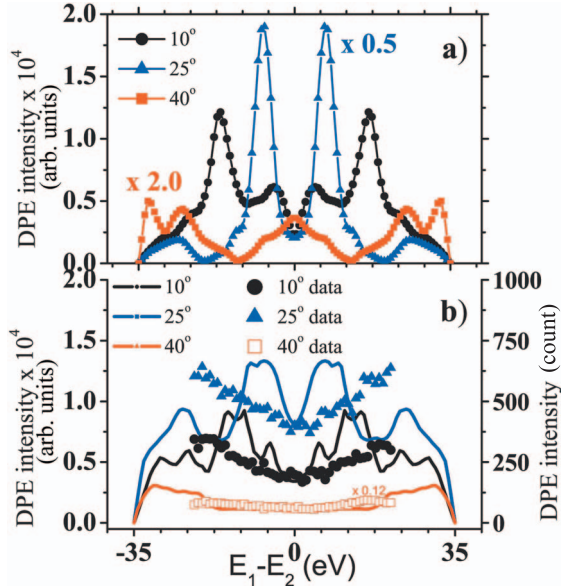


FIG. 8. (Color) The $(\gamma, 2e)$ energy sharing probability: (a) cuts through the 2D intensity map at $\theta = 10^\circ, 25^\circ,$ and 40° ; (b) sharing distributions same as in (a) additionally averaged over the azimuthal angle ($\Delta\phi = 20^\circ$), polar angle ($\Delta\theta = 5^\circ$), and kinetic energy ($\Delta E_{1,2} = 2$ eV) according to the typical experimental uncertainty values. Included are also the experimental results.

mated by its form in the long-wavelength limit and results in a generic dependence of the computed spectra on the energies and the emission directions of the photoelectrons. This model is supposed to describe only elastic two electron ionization so that energy-loss processes are not included and their contribution to the DPE signal can be a source of difference between theory and experiment. Here, we present calculations for the photon energy 50 eV. The sum energy is $E_1 + E_2 = 35$ eV. These values correspond to the peak position in experimental spectrum shown in Fig. 2. The involved initial electronic states are in the energy window E_F to $E_{\min} = E_F - 5$ eV, which covers most of the Cu(111) d band. To contrast photoemission from the d band with that from surface states, a better experimental resolution is needed. Theoretically, this has been done in Ref. 17. As the photoelectron energies are measured with respect to the Fermi level, we have $E_F = -5$ eV, and the energy conservation implies $E_{\text{sum}} - \omega = E_F + E_{\min}$. The sum energy of the pair is then between $E_{\text{sum}} = 30$ and 40 eV (constant sum energies are indicated by the dashed diagonal line in Fig. 4).

In Fig. 8(a) we present theoretical energy sharing distributions at three different angles: $\theta_{1,2} = 10^\circ, 25^\circ, 40^\circ$. Here the symmetric coplanar geometries $\theta_1 = -\theta_2 = \theta$ and $\phi_1 = \phi_2 = 0$ (Fig. 1, upper scheme) are used. To account for experimental uncertainty in angles and energies, we performed additional calculations and then average them within the domain $\Delta\theta = 5^\circ$, $\Delta\phi = 20^\circ$, and $\Delta E = 2$ eV [Fig. 8(b)]. Inspection of averaged distributions demonstrates that first the intensity grows upon increase in interelectron angle (cf. 10° and 25° curves) because very small angles are suppressed by the Coulomb repulsion. Further increase in angle (cf. 25° and 40°) leads to the intensity falloff. In our model this effect is explainable in terms of strong directional depen-

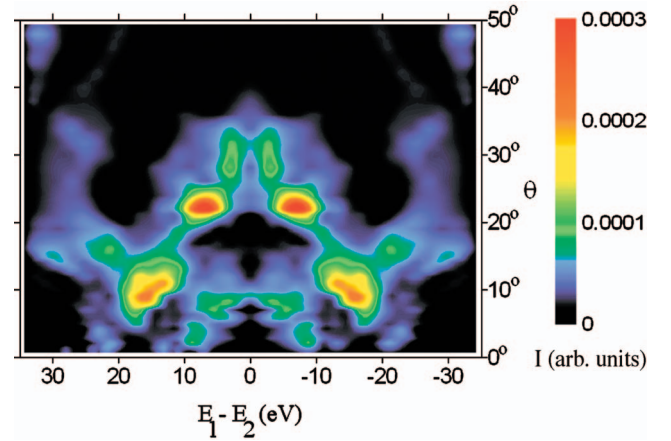


FIG. 9. (Color) The $(\gamma, 2e)$ energy-angular correlation map: the intensity (color line) as a function of the energy sharing ($E_1 - E_2$) and the angle between ejected electrons. The Cartesian coordinates are specified according to Fig. 1 so that y axis is normal to the surface and yz plane is a mirror plane. The photon energy is 50 eV, normal incidence, and is linearly polarized along x . The detection geometry is coplanar symmetric: electrons are emitted in xy plane, their polar angles are kept equal, $\theta_1 = -\theta_2 = \theta$, and serve as a vertical coordinate of the plot.

dence of ee interaction: at large angles electrons become nearly independent and hence the DPE probability rapidly decreases.

Another observation is that strong repulsion at small angles prevents equal energy sharing between electrons. This is reflected, for example, in the shift of the position of the main intensity peaks in Fig. 8(a) and 8(b) for $\theta = 10^\circ$ and $\theta = 25^\circ$; while at 25° electrons have almost the same kinetic energies, at 10° their energies tend to relate approximately as 1 is to 2.5. However, this is only a simple hand-waving argument, whereas the detailed structure of the distributions depends on the peaked structure of the k -resolved density of initial electronic states, as well as on the scattering on the lattice. As for the detailed comparison with the measured values, we concluded that a definitive statement should await further progress in refining the experimental resolution.

To present a more extensive analysis of the electronic correlation in DPE process, we calculate the full set of energy sharing distributions at constant total energy $E_1 + E_2 = 35$ eV for all possible interelectron angles. Again, we chose the symmetric coplanar geometries $\theta_1 = -\theta_2 = \theta$ and $\phi_1 = \phi_2 = 0$ (Fig. 1, upper scheme). Data are arranged in a form of the 2D map where the horizontal coordinate is again the energy difference ($E_1 - E_2$) in electron volt and the vertical coordinate is angle θ . The pattern in Fig. 9 shows that in the present model the appreciable DPE intensity can be expected up to the values of $\theta \approx 40^\circ$ (80° between electrons). In general, we also observe a weak intensity for less correlated geometries, i.e., very large mutual angles of very asymmetric energy sharing. On the other hand the pair correlation carves a hole (the exchange and correlation hole) in the DPE intensity when the two electrons are emitted in close vicinity in momentum space. What we observe in Fig. 9 is, however, a structured hole. This is a result of two further factors: When varying θ or $E_1 - E_2$ one scans through the (two particle)

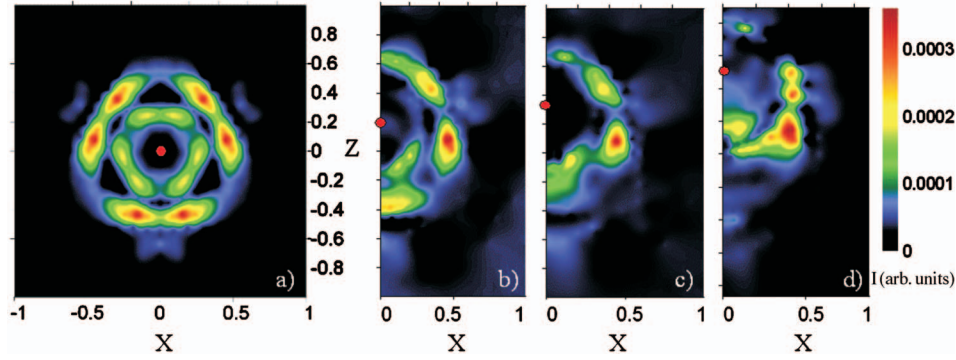


FIG. 10. (Color) The $(\gamma, 2e)$ angular distributions for the pair of slow (12 eV) and fast (23 eV) electrons projected on the normalized surface-parallel momentum plane xz . The photon energy is $\hbar\omega=50$ eV, normal incidence, p polarized. Fast electron is fixed in the position of the red spot. In panel (a) we show the full 2D momentum distribution if the fixed electron is at $X=Z=0$. Panels (b)–(d) show the resulting distribution if the fixed electron moves along Z direction: $Z=0.2, 0.3,$ and 0.5 while keeping $X=0$.

initial momentum spectral density of the surface whose peaked structures are then reflected in the DPE intensity. In addition, the emitted electrons experience strong diffraction from the lattice, depending on their wave vectors and the crystal orientation. Energy-angular correlation map in Fig. 9 yields an estimate for the extent of correlation angle (the interelectron angle most favorable for the DPE events, also identified with the radius of the so-called Coulomb correlation hole). Choosing, for example, a pair of electrons with $E_1=10$ eV and $E_2=25$ eV, we find that maximal intensity for $\Delta E=15$ eV corresponds to the relative angle $\theta_1+\theta_2=20^\circ$. Combination of closer kinetic energies $E_1=20$ eV and $E_2=15$ eV results in larger correlation angle $\theta_1+\theta_2=45^\circ$.

To compare with the angular distributions shown in Fig. 7, we plot (Fig. 10) the DPE intensity as a function of the emission direction of one electron. Both kinetic energies and the emission direction of the second electron are fixed. The DPE intensity depends on angular coordinates according to two opposite trends. Interelectron angle has to be small enough to provide sufficiently strong interaction. On the other hand, this angle cannot be very small because of the Coulomb repulsion. Competition between these trends explains the depletion region and then the cloud of high coincidence signal around the position of the fixed electron (depicted by the full red circle Fig. 10). The threefold surface symmetry becomes apparent in the DPE intensity for high symmetric scattering geometry (left panel in Fig. 10). Going away from such symmetric situation (moving the fixed electron along z axis), the intensity circle becomes nonsymmetric and its shape is determined in a nontrivial manner by diffraction, correlation, and initial-state spectral density effects. These trends are also confirmed by another theoretical approach.¹⁸

VI. SUMMARY AND FINAL REMARKS

We have studied the process of electron pair emission from a Cu(111) surface. We excited the specimen with 50 eV

photons. We found that the pair emission shows a prominent contribution from the Cu $3d$ states. Most of this intensity is found for unequal energies of the electrons and a large angle between the trajectories. Participation of surface states could not be identified. Experiments with different photon energies may enhance the contribution of the surface state compared to the bulk states. Theoretical calculations support the first trend about unequal energy sharing but give a lower estimate for the angle at which the emission intensity is maximal.¹⁹ We illustrate this by the energy-angular correlation map, which allows us to trace spatial and energy aspects of $(\gamma, 2e)$ process simultaneously on the same plot. The momentum distribution of the coincidence intensity revealed that the depletion zone around the fixed emission direction of one electron can be fully mapped. The origin of this is due to the xc hole. In this context it is worthwhile to mention the relation to the two-particle intensity interferometry experiments based on the Hanbury Brown–Twiss effect,^{20–23} which leads to enhanced or decreased (also called bunching or antibunching) detection probability of respectively two close bosons or fermions. This phenomena relies purely on the symmetry and shows up for noninteracting quantum particles, e.g., photons or neutral atoms. In our experiment (and theory) this effect is present and shows up as a part of the exchange hole. On the other hand, as we demonstrated above, our spectra are dominated in addition by the interparticle interaction. A separation between the spin-induced and the Coulomb-induced features in the spectra entails the use of spin-resolved detectors. Developments in this direction are currently under way.

ACKNOWLEDGMENTS

We thank the staff of the BESSY II storage ring for the excellent support. Furthermore we wish to thank H. Engelhard and D. Hartung for their skillful work in constructing the apparatus. This work was supported by the DFG through SFB 762.

- ¹E. Wigner and F. Seitz, *Phys. Rev.* **43**, 804 (1933).
- ²J. C. Slater, *Rev. Mod. Phys.* **6**, 209 (1934).
- ³P. Fulde, *Electron Correlations in Molecules and Solids*, Springer Series in Solid State Sciences Vol. 100 (Springer, Berlin, 1993).
- ⁴K. Byczuk, M. Kollar, K. Held, Y.-F. Yang, I. A. Nekrasov, T. Pruschke, and D. Vollhardt, *Nat. Phys.* **3**, 168 (2007), and references therein.
- ⁵J. Berakdar, *Phys. Rev. B* **58**, 9808 (1998).
- ⁶N. Fominykh, J. Berakdar, J. Henk, and P. Bruno, *Phys. Rev. Lett.* **89**, 086402 (2002).
- ⁷H. W. Biester, M. J. Besnard, G. Dujardin, L. Hellner, and E. E. Koch, *Phys. Rev. Lett.* **59**, 1277 (1987).
- ⁸R. Herrmann, S. Samarin, H. Schwabe, and J. Kirschner, *Phys. Rev. Lett.* **81**, 2148 (1998).
- ⁹J. Berakdar, S. N. Samarine, R. Herrmann, and J. Kirschner, *Phys. Rev. Lett.* **81**, 3535 (1998); J. Berakdar, *Phys. Rev. A* **56**, 370 (1997).
- ¹⁰F. U. Hillebrecht, A. Morozov, and J. Kirschner, *Phys. Rev. B* **71**, 125406 (2005).
- ¹¹F. O. Schumann, C. Winkler, G. Kerherve and J. Kirschner, *Phys. Rev. B* **73**, 041404(R) (2006).
- ¹²F. O. Schumann, C. Winkler, and J. Kirschner, *New J. Phys.* **9**, 372 (2007).
- ¹³S. G. Louie, P. Thiry, R. Pinchaux, Y. Petroff, D. Chandesris, and J. Lecante, *Phys. Rev. Lett.* **44**, 549 (1980); J. A. Knapp, F. J. Himpsel, and D. E. Eastman, *Phys. Rev. B* **19**, 4952 (1979); S. D. Kevan, *Phys. Rev. Lett.* **50**, 526 (1983).
- ¹⁴J. Berakdar, H. Gollisch, and R. Feder, *Solid State Commun.* **112**, 587 (1999).
- ¹⁵N. Fominykh, J. Henk, J. Berakdar, P. Bruno, H. Gollisch, and R. Feder, *Solid State Commun.* **113**, 665 (2000).
- ¹⁶N. Fominykh, J. Henk, J. Berakdar, and P. Bruno, in *Correlations, Polarization, and Ionization in Atomic Systems*, edited by D. H. Madison and M. Schulz (AIP, Melville, NY, 2002), pp. 210–216.
- ¹⁷N. Fominykh and J. Berakdar, *J. Electron Spectrosc. Relat. Phenom.* **161**, 125 (2007).
- ¹⁸H. Gollisch, N. v. Schwartzberg, and R. Feder, *Phys. Rev. B* **74**, 075407 (2006).
- ¹⁹F. O. Schumann, J. Kirschner, and J. Berakdar, *Phys. Rev. Lett.* **95**, 117601 (2005).
- ²⁰R. Hanbury-Brown and R. Q. Twiss, *Nature (London)* **178**, 1046 (1956).
- ²¹D. H. Boal, C. K. Gelbke, and B. K. Jennings, *Rev. Mod. Phys.* **62**, 553 (1990).
- ²²H. Kiesel, A. Renz, and F. Hasselbach, *Nature (London)* **418**, 392 (2002).
- ²³T. Jeltos, J. M. McNamara, W. Hogervorst, W. Vassen, V. Krachmalnicoff, M. Schellekens, A. Perrin, H. Chang, D. Boiron, A. Aspect, and C. I. Westbrook, *Nature (London)* **445**, 402 (2007).